Citation: G. López-Nicolás, C. Sagüés. Vision-based exponential stabilization of mobile robots. Autonomous Robots, vol. 30, pp. 293-306, 2011

Vision-Based Exponential Stabilization of Mobile Robots

G. López-Nicolás and C. Sagüés
Instituto de Investigación en Ingeniería de Aragón
Universidad de Zaragoza, Spain.
gonlopez@unizar.es, csagues@unizar.es

***Abstract*—A new smooth closed loop time invariant control law is proposed for the exponential stabilization of mobile robots with nonholonomic motion constraints. The control scheme relies solely on visual information and includes an observer for the system state estimation by means of the essential matrix. The problem of model degeneracies due to short baseline is solved with the definition of a virtual target that provides a stable estimation of the essential matrix. The novelty of this paper lies in the new vision-based control scheme with state observer which is robust, ensuring convergence to the target location. The stability of the system under the proposed control law is demonstrated and experimental results show the goodness of the approach.**

Keywords*—Visual control, Essential matrix, Nonholonomic mobile robots.

I. Introduction

Visual information has been extensively used for robot localization, navigation and control. Visual control is an extensive field of research in the design of motion controllers and it has focused the attention of many researchers [1] [2]. In general, visual control in mobile navigation refers to the pose control of a vehicle in a closed loop using the input of a visual sensor. We present a new approach to solve the problem of pose stabilization of a robot by means of a state feedback control law that relies on vision information. The system consists of a mobile robot with a calibrated camera mounted onboard, and a goal defined by a reference image taken at the target location. The problem tackled is to design a visual control that autonomously drives the robot to the goal by using only the visual information.

There are some related works on control. The piecewise smooth controller proposed in [3] has the characteristic of not requiring infinite switching like other approaches, such as the sliding mode controller. In [4], with a particular choice of the system state variables, global stability properties are guaranteed by smooth feedback control law. This is suitable to be used for steering, path following, and navigation. The control law there allows forward and backward motions, whereas in [5], the vehicle is requested to move only in the forward direction, avoiding cusps in the paths by using a Lyapunov-like based design for the control law. The discontinuous, bounded, time invariant, state feedback control law proposed in [6] is able to drive the robot to the target position without reversing direction of its motion (forward or backward), and moving along smooth paths. In [7], the pose of the mobile robot with respect to a generic rigid object is controlled using image-based visual feedback, and an adaptive control law is proposed in the case of unknown height of the object points. Our proposal presents a different control law that is exponentially stable, and it is designed within a control scheme that includes a visual perception procedure.

The problem of steering the robot to a target location can be solved as a homing task defined directly on image features [8], [9]. These approaches are usually simple and efficient but their robustness directly depends on the performance of the features. The robustness can be improved if the image information extracted is filtered through the constraints imposed by the geometric model across the views. Some traditional visual control approaches are based on the epipolar geometry [10]–[12], but this model degenerates with short baseline. So, as the robot approaches to the target, the epipolar geometry becomes unstable. This problem has been solved using auxiliary procedures at the last stage of the motion [13]. However, it would be better to avoid the need of switching the model in favor of robustness and simplicity. A good alternative is the homography-based approach [14]–[19]. However, if no plane is detected, the homography-based control fails. This problem was solved through virtual planes [20], although in general, estimations based on virtual planes with wide baseline are not robust to mismatches, noise or occlusions. Here, we propose a new method using the classic epipolar geometry but addressing its drawbacks.

The computation of the essential matrix using the general method with eight points [21] becomes ill-conditioned with planar scenes. This issue has been addressed by using a minimum set of five points and the intrinsic camera calibration [22]. A well known problem related with the epipolar geometry is that this model becomes undefined when there is no translation between the images (current and target). This results in a poor and unstable estimation of the essential matrix with short baseline. Instead of switching to another control law we propose a novel approach avoiding short baseline degeneracies. For this purpose we define a virtual target taking advantage of the planar motion constraint as presented in [23]. The virtual target is generated from the visual information of the current and target images and it is defined out of the motion plane and vertically with respect to the target. This procedure relies on the epipolar transfer properties. The essential matrix computed across the current image and the virtual target is always well defined despite short baseline, allowing a stable state estimation.

The approach proposed takes advantage of techniques of control theory and two-view geometry from computer vision. Our proposed control scheme is novel in that it processes the visual information through the classical epipolar geometry but solving its well known problems. An observer of the

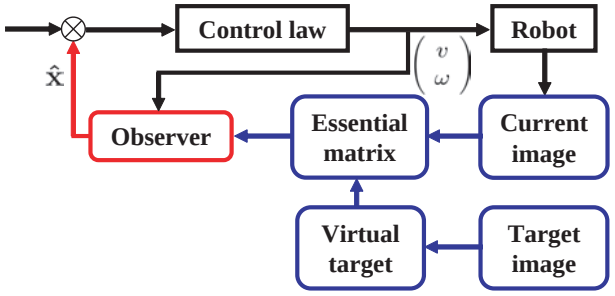

Fig. 1. Overview of the control loop. Image features are extracted and matched between the image taken at the current location and the virtual target image. The essential matrix is then estimated from the set of matches. The observer estimates the state of the system and the control law gives the velocities that lead the robot to the target location.

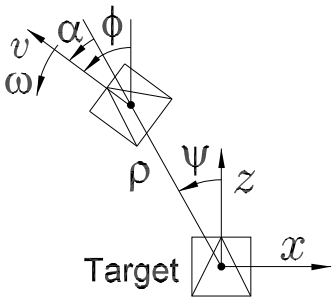

Fig. 2. Cartesian and polar coordinate systems in the target location.

robot state based on visual information through the essential matrix has been designed for the adaptive estimation of the system state which makes the full system to behave robustly during the trajectory. Moreover, the stability of the system is also demonstrated when there is uncertainty in the system parameters.

An overview of the control scheme is shown in Fig. 1. The control law is presented in Section II. The visual perception procedure and the state observer are described in Sections III and IV, respectively. Experimental results are presented in Section V, and conclusions are given in Section VI.

II. Control Scheme

A. System model

The system to be controlled is a nonholonomic robot whose model together with the sensory system is expressed in a general way as

$$\begin{cases} \dot{\mathbf{x}} &= \mathbf{g}(\mathbf{x},\mathbf{u}) \\ \mathbf{y} &= \mathbf{h}(\mathbf{x}) \end{cases} \tag{1}$$

where $\mathbf{x}(t)$ denotes the state vector in Cartesian $(x(t), z(t), \phi(t))^T$ or polar $(\rho(t), \alpha(t), \phi(t))^T$ coordinates, $\mathbf{u}(t)$ the system input vector consisting of the linear velocity $v(t)$ and angular velocity $\omega(t)$, and $\mathbf{y}(t)$ the output vector. The coordinate system is illustrated in Fig. 2. The kinematics of a unicycle robot can be expressed in Cartesian coordinates as a function of the robot state and input velocities by

$$\begin{pmatrix} \dot{x} \\ \dot{z} \\ \dot{\phi} \end{pmatrix} = \begin{bmatrix} -\sin\phi & 0 \\ \cos\phi & 0 \\ 0 & 1 \end{bmatrix} \begin{pmatrix} v \\ \omega \end{pmatrix} . \tag{2}$$

Traditionally, mobile robots have been modeled in Cartesian coordinates. However, it has been shown (e.g. [4], [5], [6]) that using polar coordinates may solve the problem contained in the Theorem of Brockett [24] for the system stabilization, allowing to design exponentially stabilizing, smooth, state feedback control laws. Thus, the expressions in (2) are converted to polar coordinates, being

$$x = -\rho\sin\psi \quad \text{and} \quad z = \rho\cos\psi \, . \tag{3}$$

The alignment error $\alpha(t)$ is defined as the angle between the robot body z-axis and the distance vector ρ,

$$\alpha = \phi - \psi \, . \tag{4}$$

The kinematics of the system can be then expressed as

$$\begin{pmatrix} \dot{\rho} \\ \dot{\alpha} \\ \dot{\phi} \end{pmatrix} = \begin{bmatrix} \cos\alpha & 0 \\ -\frac{1}{\rho}\sin\alpha & 1 \\ 0 & 1 \end{bmatrix} \begin{pmatrix} v \\ \omega \end{pmatrix} . \tag{5}$$

B. Control Law

In this section we describe the proposed control law. The input velocities of the system are defined as a function of the state variables as follows,

$$v = -k_\rho\,\rho\,\cos\alpha \tag{6}$$
$$\omega = -k_\alpha\,\alpha + k_\phi\,\phi \tag{7}$$

where k_ρ, k_α, and k_ϕ are positive constant gains of the control. The constraints on these gains that make the control stable are analyzed later. Introducing in (5) the input velocities just defined, we obtain a closed-loop system described by equations of the form

$$\begin{aligned} \dot{\rho} &= -k_\rho\,\rho\,\cos^2\alpha \\ \dot{\alpha} &= k_\rho\,\sin\alpha\,\cos\alpha\, - k_\alpha\,\alpha + k_\phi\,\phi \\ \dot{\phi} &= -k_\alpha\,\alpha + k_\phi\,\phi \end{aligned} \tag{8}$$

Some examples of the evolution of the system under the control velocities (6) and (7) are given in Fig. 3. The initial locations are distributed around the target with initial orientation 0 or $\pi/2$, while the target is located in $(\rho,\alpha,\phi)^T = (0,0,0)^T$ (Fig. 3 (left)). The robot reaches properly the target, although some trajectories are not visually appealing, in particular those in which the robot starts behind the target location. We define the alternative but equivalent target location $(0,\pi,-\pi)^T$, complementing the previous case as can be seen in Fig. 3 (right). While this alternative target trivially corresponds to the same desired position and orientation of the robot, it results in a different way of reaching the target. Thus, selecting initially one of the equivalent targets we avoid trajectories with several cusps. To do it, we redefine the angular velocity of the control (7) as

$$\omega = -k_\alpha\,(\alpha - \alpha^*) + k_\phi\,\phi \, , \tag{9}$$

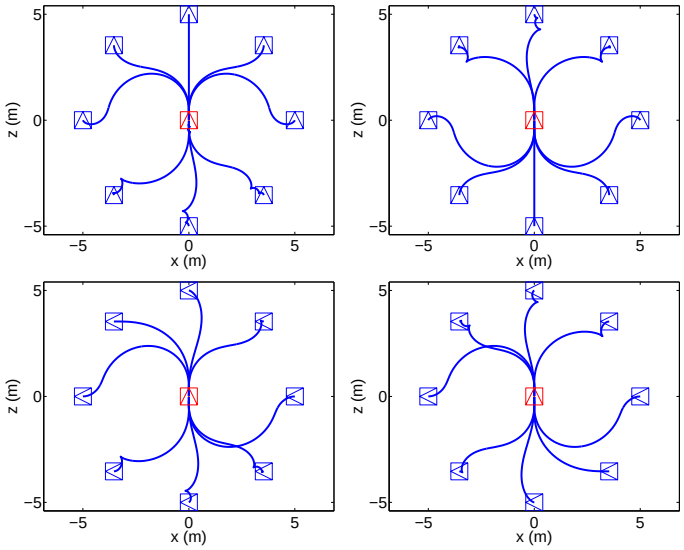

Fig. 3. Simulations for different initial locations with $\phi(t=0)=0$ (first row) and $\phi(t=0)=\pi/2$ (second row). The target is $(0,0,0)^T$ (i.e. $\alpha^*=0$) and $(0,\pi,-\pi)^T$ (i.e. $\alpha^*=\pi$) in the left and right columns, respectively.

where $\alpha^*=0$ if $|\psi(0)|\leq\pi/2$ with $\alpha\in[-\pi,\pi]$, or $\alpha^*=\pi$ if $|\psi(0)|>\pi/2$ with $\alpha\in[0,2\pi]$. Hereafter, we consider without loss of generality $\alpha^*=0$, being the subsequent analysis analogue for the case of $\alpha^*=\pi$.

C. Stability Analysis of the control law

We study the stability of the closed-loop system under the input control velocities previously defined (8).

Proposition 2.1 (Local exponential stability): The closed-loop system (8) is locally exponentially stable if and only if $(k_\alpha - k_\phi - k_\rho) > 0$.

Proof: The linear approximation of the sinusoidal functions that appear in our system can be written as $\sin\alpha = \alpha + h.o.t.$ and $cos\alpha = 1 + h.o.t.$ (where $h.o.t.$ stands for high order terms). Then, the linear approximation of the system is

$$\begin{pmatrix}\dot\rho\\ \dot\alpha\\ \dot\phi\end{pmatrix} = \begin{bmatrix}-k_\rho & 0 & 0\\ 0 & k_\rho - k_\alpha & k_\phi\\ 0 & -k_\alpha & k_\phi\end{bmatrix}\begin{pmatrix}\rho\\ \alpha\\ \phi\end{pmatrix} + h.o.t. \quad (10)$$

This system is locally exponentially stable if and only if the eigenvalues of the linearized system matrix are negative. The eigenvalues are obtained solving the characteristic equation

$$(\lambda + k_\rho)\left(\lambda^2 + (k_\alpha - k_\phi - k_\rho)\lambda + k_\rho\, k_\phi\right) = 0 \quad (11)$$

yielding that $Re(\lambda) < 0$ if

$$k_\alpha - k_\phi - k_\rho > 0 \quad (12)$$

The control gains are positive by definition and the local exponential stability is guaranteed if the selected control gains hold (12). ■

Proposition 2.2 (Global asymptotic stability): The closed-loop system (8) with the control gains selected following (12) is globally asymptotically stable if

$$k_\alpha - 2\,k_\phi > 0\,. \quad (13)$$

Proof: In the following, the stability of the control scheme is analyzed by means of the *Lyapunov's Direct Method* [25]. We define the candidate Lyapunov function as

$$V(\mathbf{x}) = \mathbf{x}^T\,\mathbf{P}\,\mathbf{x} + \frac{k_\rho}{2}\,\sin^2\alpha\,, \quad (14)$$

where $V(\mathbf{x})>0$ for all $\mathbf{x}\neq 0$, with

$$\mathbf{P} = \frac{1}{2}\begin{bmatrix}1 & 0 & 0\\ 0 & k_\phi & -k_\phi\\ 0 & -k_\phi & k_\phi\end{bmatrix}\,. \quad (15)$$

The derivative of (14) yields

$$\begin{aligned}\dot V &= \rho\,\dot\rho + k_\phi(\phi-\alpha)(\dot\phi-\dot\alpha) + k_\rho\,\dot\alpha\,\sin\alpha\,\cos\alpha\\ &= -k_\rho\,\rho^2\,\cos^2\alpha \quad (16)\\ &\quad + k_\rho\,\alpha\,\sin\alpha\,\cos\alpha\left(k_\phi + k_\rho\frac{\sin\alpha\,\cos\alpha}{\alpha} - k_\alpha\right)\end{aligned}$$

It can be seen that $\dot V<0$ for all $\alpha\in(-\pi/2,\,\pi/2)$ if the following constraint holds:

$$k_\alpha - k_\phi - (k_\rho\,\sin\alpha\,\cos\alpha)/\alpha > 0\,. \quad (17)$$

Since $(\sin\alpha\,\cos\alpha)/\alpha$ is bounded by 1, constraint (17) leads to (12). We next study the case of $\alpha=\pm\pi/2$, which results in $\dot V=0$. In this case, we check the derivative of α in (8).

$$\dot\alpha(\alpha=\pm\pi/2) = \mp k_\alpha\,\pi/2 + k_\phi\,\phi\,. \quad (18)$$

We can ensure that $\dot\alpha<0$ when $\alpha=\pi/2$, and $\dot\alpha>0$ when $\alpha=-\pi/2$, if the following constraint holds:

$$-k_\alpha + \frac{2}{\pi}\,k_\phi\,\phi < 0\,,\quad k_\alpha + \frac{2}{\pi}\,k_\phi\,\phi > 0\,. \quad (19)$$

If the maximum bounds of ϕ are considered, i.e. $\phi=\pm\pi$ respectively, we obtain constraint (13). Therefore, the regulated system is asymptotically stable for all $\alpha\in[-\pi/2,\,\pi/2]$.

In order to show the region of attraction of the equilibrium $\mathbf{x}=\mathbf{0}$ is global, we also analyze the case of $\alpha\in[-\pi,-\pi/2]\cup[\pi/2,\pi]$. By checking the derivative of α in (8) we have

$$\alpha\in[\pi/2,\pi]\Rightarrow\quad \dot\alpha<0\Leftrightarrow -\tfrac{\pi}{2}\,k_\alpha + k_\phi\,\phi<0\,, \quad (20)$$

$$\alpha\in[-\pi,-\pi/2]\Rightarrow\quad \dot\alpha>0\Leftrightarrow \tfrac{\pi}{2}\,k_\alpha + k_\phi\,\phi>0\,. \quad (21)$$

where the most unfavorable case of α is used. These previous constraints yields to constraint (13) when the maximum bounds of ϕ are included. Thus, the global asymptotic stability of the regulated system (8) is guaranteed if constraints (12) and (13) holds. ■

III. Visual Perception

An overview of the visual perception system within the control scheme is shown in Fig. 1. Features are extracted and matched between the image taken at the current location and the virtual target image. The essential matrix $\mathbf{E}(t)$ is estimated from the set of matches and the intrinsic camera calibration parameters.

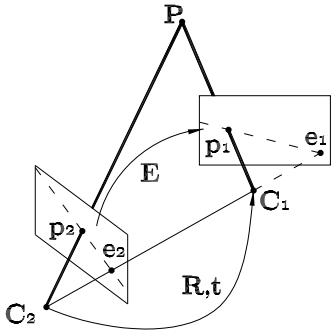

Fig. 4. Essential matrix relating two views. The camera optical centers are $\mathbf{C}_1$ and $\mathbf{C}_2$. A 3D point $\mathbf{P}$ is projected in the images as $(\mathbf{p}_1, \mathbf{p}_2)$. The epipoles ($\mathbf{e}_1$ and $\mathbf{e}_2$) are the intersections of the baseline (the line joining the optical centers of the cameras $\overline{\mathbf{C}_1\mathbf{C}_2}$) with the image planes.

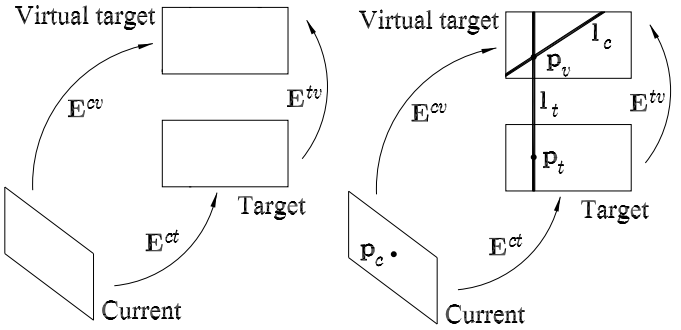

Fig. 5. (Left) Essential matrices across the views. The virtual target is defined above the target. (Right) A 3D point is projected into the three views as $(\mathbf{p}_c, \mathbf{p}_t, \mathbf{p}_v)$. The value of $\mathbf{p}_v$ is computed by means of the epipolar transfer.

A. The Essential Matrix

Consider the geometry of the camera to be modeled by perspective projection; and let us suppose two images obtained with the same camera. The essential matrix across the views (Fig. 4) is defined as

$$\mathbf{E} = [\mathbf{t}]_\times \mathbf{R} = \begin{bmatrix} 0 & -t_z & t_y \\ t_z & 0 & -t_x \\ -t_y & t_x & 0 \end{bmatrix} \mathbf{R}\,, \qquad (22)$$

being $\mathbf{R}$ the rotation and $\mathbf{t} = (t_x, t_y, t_z)^T$ the translation between the cameras. The essential matrix can be related with the fundamental matrix with $\mathbf{E} = \mathbf{K}^T\mathbf{F}\mathbf{K}$, being $\mathbf{K}$ the internal camera calibration [21]. It can be computed by solving a linear system from a set of point correspondences between the two views [21].

We assign the coordinate system to the target location as shown in Fig. 2, where the camera optic axis coincides with the z-axis of the robot frame. As previously described, the configuration of the robot system is given by $\mathbf{x} = (\rho, \alpha, \phi)^T$. The framework considered in our approach consists of the target image taken at the desired location (i.e. at $\mathbf{x} = (0,0,0)^T$, with $y = 0$, being y the vertical coordinate), the current image (at $\mathbf{x} = (\rho, \alpha, \phi)^T$, with $y = 0$) and a generated virtual target image (at $\mathbf{x} = (0,0,0)^T$, with $y = Y = cte \neq 0$). These images are denoted as c (current), t (target) and v (virtual target). This framework is shown in Fig. 5 (left), where the essential matrices across the images are denoted as $\mathbf{E}^{ct}$, $\mathbf{E}^{tv}$ and $\mathbf{E}^{cv}$. The essential matrix $\mathbf{E}^{cv}$ relating the current and virtual images can be parameterized up to scale using

$$\mathbf{R}^{cv} = \begin{bmatrix} \cos\phi & 0 & -\sin\phi \\ 0 & 1 & 0 \\ \sin\phi & 0 & \cos\phi \end{bmatrix},\ \mathbf{t}^{cv} = -\begin{pmatrix} -\rho\sin\psi \\ Y \\ \rho\cos\psi \end{pmatrix}$$

with (22) as

$$\mathbf{E}^{cv} = \begin{bmatrix} -Y\sin\phi & -\rho\cos\psi & -Y\cos\phi \\ \rho\cos\alpha & 0 & -\rho\sin\alpha \\ Y\cos\phi & \rho\sin\psi & -Y\sin\phi \end{bmatrix}. \qquad (23)$$

B. Definition of the Virtual Target

We need first to define the virtual target from the information available: the current and target images. The virtual target is defined at the beginning of the navigation (i.e. at $t = 0$). The idea is to generate the virtual target using the epipolar transfer across the three images [21]. For this purpose we need to compute the three essential matrices (Fig. 5 (left)). $\mathbf{E}_0^{ct}$, where subindex denotes $t = 0$, is estimated from the correspondences between the current and target images and $\mathbf{E}^{tv}$ is obtained and normalized in the target location $(0,0,0)$ up to a constant height $y = Y$ as

$$\mathbf{E}^{tv} = \begin{bmatrix} 0 & 0 & 1 \\ 0 & 0 & 0 \\ -1 & 0 & 0 \end{bmatrix}. \qquad (24)$$

On the other hand, the matrix $\mathbf{E}_0^{ct}$ can be parameterized up to an unknown scale factor from (22) with $y = 0$ and normalized with

$$\rho_0 = sign(E_{12}^{ct})\sqrt{(E_{12}^{ct})^2 + (E_{32}^{ct})^2} \qquad (25)$$

giving

$$\mathbf{E}_0^{ct} = \begin{bmatrix} 0 & \cos\psi_0 & 0 \\ \cos\alpha_0 & 0 & -\sin\alpha_0 \\ 0 & \sin\psi_0 & 0 \end{bmatrix}, \qquad (26)$$

from which the following expression can be derived:

$$\tan\phi_0 = \frac{E_{21}^{ct}E_{32}^{ct} - E_{12}^{ct}E_{23}^{ct}}{E_{12}^{ct}E_{21}^{ct} + E_{23}^{ct}E_{32}^{ct}}\,. \qquad (27)$$

Note that ρ_0 is never zero except if the initial position is in the target location. We can write (23) to be compared with (26) as

$$\mathbf{E}_0^{cv} = \begin{bmatrix} \frac{-Y\sin\phi_0}{\rho_0} & \cos\psi_0 & \frac{-Y\cos\phi_0}{\rho_0} \\ \cos\alpha_0 & 0 & -\sin\alpha_0 \\ \frac{Y\cos\phi_0}{\rho_0} & \sin\psi_0 & \frac{-Y\sin\phi_0}{\rho_0} \end{bmatrix}. \qquad (28)$$

Entries E_{12}^{cv}, E_{21}^{cv}, E_{22}^{cv}, E_{23}^{cv} and E_{32}^{cv} are known, as they are the same as the corresponding entries of (26). Entries E_{11}^{cv}, E_{13}^{cv}, E_{31}^{cv} and E_{33}^{cv} depend on ϕ_0, which is obtained from (27), and Y/ρ_0. We do not know ρ_0 (because of the unknown scale) and we do not care about Y except it is not equal to zero.

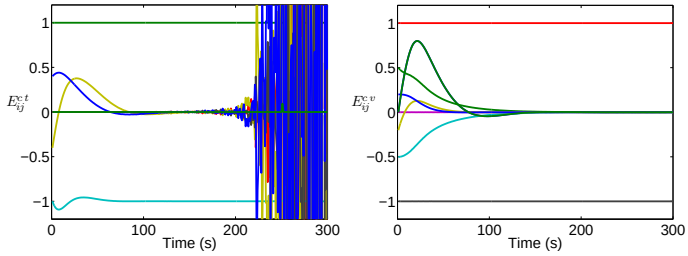

Fig. 6. Evolution of the essential matrix entries of $\mathbf{E}^{ct}$ (left) and using the virtual target $\mathbf{E}^{cv}$ (right) during a simulation in which the robot is led to the target location. They show the performance of the model with short baseline at the end of the motion.

Then, we can assign Y/ρ_0 an arbitrary value (not equal to zero) determining $\mathbf{E}_0^{cv}$. In practice, a good option is to select Y in the same order of magnitude as the initial ρ_0, i.e. $Y = \rho_0$, and so $Y/\rho_0 = 1$.

We know the three essential matrices $\mathbf{E}_0^{ct}$, $\mathbf{E}^{tv}$ and $\mathbf{E}_0^{cv}$ relating the three views and we can apply the epipolar transfer to generate the virtual target (Fig. 5 (right)). Let us consider $\mathbf{p}_c$ and $\mathbf{p}_t$ two corresponding points in the current and target images, respectively. The objective is to find the corresponding point in the virtual image. The required point $\mathbf{p}_v$ matches point $\mathbf{p}_c$ in the current image and $\mathbf{p}_t$ in the target image. Therefore, it must lie on the epipolar lines corresponding to $\mathbf{p}_c$ and $\mathbf{p}_t$. These epipolar lines $\mathbf{l}_c$ and $\mathbf{l}_t$ can be computed since the matrices $\mathbf{E}_0^{cv}$ and $\mathbf{E}^{tv}$ are known:

$$\mathbf{p}_c^T \mathbf{E}_0^{cv} \mathbf{p}_v = 0 \quad \Rightarrow \quad \mathbf{l}_c^T = \mathbf{p}_c^T \mathbf{E}_0^{cv} \, . \tag{29}$$

$$\mathbf{p}_t^T \mathbf{E}^{tv} \mathbf{p}_v = 0 \quad \Rightarrow \quad \mathbf{l}_t^T = \mathbf{p}_t^T \mathbf{E}^{tv} \, . \tag{30}$$

The required point $\mathbf{p}_v$ is the intersection of the epipolar lines

$$\mathbf{p}_v = \mathbf{l}_c \times \mathbf{l}_t = \left((\mathbf{E}_0^{cv})^T \mathbf{p}_c \right) \times \left((\mathbf{E}^{tv})^T \mathbf{p}_t \right) \, . \tag{31}$$

This procedure is repeated for all the correspondences between the current and the target image at the beginning of the navigation. Thus, the virtual target image is defined with these computed points. This virtual target allows to compute $\mathbf{E}^{cv}(t)$ along the navigation to be used in the control law. Note that control performance depends on the quality of the estimated virtual target at $t = 0$. The advantage of using this virtual target is that $\mathbf{E}^{cv}$, unlike $\mathbf{E}^{ct}$, is well defined as the current image approaches to the target and the baseline between them reaches zero. Therefore, the problem of short baseline degeneracies is avoided. This is illustrated in the example depicted in Fig. 6.

IV. State Estimation and Nonlinear Observer

A. State Computation

The state of the robot $\mathbf{x} = (\rho, \alpha, \phi)^T$ can be computed from the essential matrix $\mathbf{E}^{cv}$. We first normalize the essential matrix up to a fixed, although unknown, scale. $\mathbf{E}^{cv}$ can be normalized by E_{13}^{cv} except when $|\phi| = \pi/2$, and in that case we can normalize by E_{11}^{cv} and we have

$$\mathbf{E} = \begin{cases} \mathbf{E}^{cv}/E_{13}^{cv} & \text{if } |\phi| \neq \frac{\pi}{2} \\ \mathbf{E}^{cv}/E_{11}^{cv} & \text{if } |\phi| = \frac{\pi}{2} \end{cases} \tag{32}$$

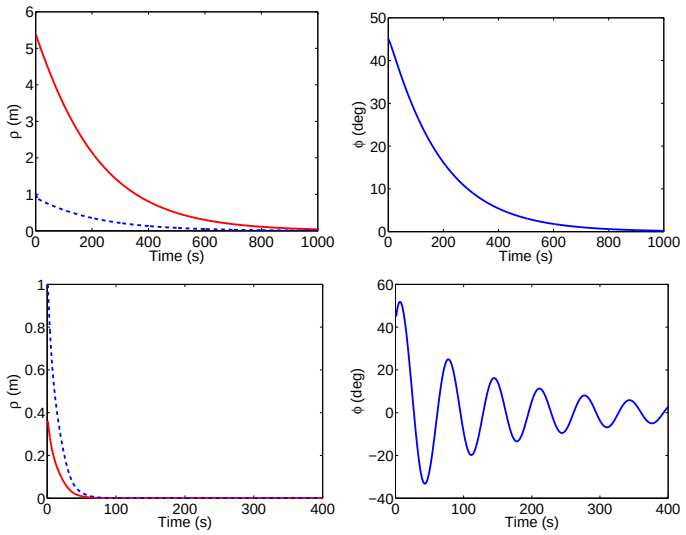

Fig. 7. Simulations without observer for initial positions (x, z, ϕ) at $(-2, 5, 45°)$ (first row) and $(-0.2, 0.3, 45°)$ (second row). Left: Evolution of the real value of ρ (solid line) and the value used in the control (dashed line). Right: Evolution of ϕ.

Where we denote $\mathbf{E}$ the normalized essential matrix $\mathbf{E}^{cv}$ with

$$\mathbf{E} = \frac{\mathbf{E}^{cv}}{E_{13}^{cv}} = \begin{bmatrix} \tan\phi & \frac{-\rho\cos\psi}{Y\cos\phi} & 1 \\ \frac{\rho\cos\alpha}{Y\cos\phi} & 0 & \frac{-\rho\sin\alpha}{Y\cos\phi} \\ -1 & \frac{-\rho\sin\psi}{Y\cos\phi} & \tan\phi \end{bmatrix} \text{ if } |\phi| \neq \frac{\pi}{2} \tag{33}$$

$$\mathbf{E} = \frac{\mathbf{E}^{cv}}{E_{11}^{cv}} = \begin{bmatrix} 1 & \frac{-\rho\cos\psi}{Y\sin\phi} & \frac{1}{\tan\phi} \\ \frac{\rho\cos\alpha}{Y\sin\phi} & 0 & \frac{-\rho\sin\alpha}{Y\sin\phi} \\ \frac{-1}{\tan\phi} & \frac{-\rho\sin\psi}{Y\sin\phi} & 1 \end{bmatrix} \text{ if } |\phi| = \frac{\pi}{2} \tag{34}$$

The current epipole $\mathbf{e}_c$ and virtual target epipole $\mathbf{e}_v$ are given by the null space $\mathbf{E}^{cv}\,\mathbf{e}_c = \mathbf{0}$ and $\mathbf{e}_v^T\,\mathbf{E}^{cv} = \mathbf{0}$. Solving for the epipoles we obtain

$$\mathbf{E}^{cv}\,\mathbf{e}_c = \mathbf{0} \quad \Rightarrow \quad \mathbf{e}_c = \left(\tan\alpha, \; \frac{Y}{\rho\cos\alpha}, \; 1 \right)^T \tag{35}$$

$$\mathbf{e}_v^T\,\mathbf{E}^{cv} = \mathbf{0} \quad \Rightarrow \quad \mathbf{e}_v = \left(-\tan\psi, \; \frac{Y}{\rho\cos\psi}, \; 1 \right)^T \tag{36}$$

From the first components of the epipoles we can directly compute α and ψ. Alternatively, we can use $\tan\alpha = -\frac{\mathbf{E}_{23}}{\mathbf{E}_{21}}$ and $\tan\psi = \frac{\mathbf{E}_{32}}{\mathbf{E}_{12}}$. Finally, the angle ϕ can be computed from (4) or (33)-(34). Notice that there is an ambiguity in the solution of the angles: (α,$\alpha + \pi$) and (ψ, $\psi + \pi$), that can be solved using a priori information (for example if the robot is initially behind or in front of the target) or using the point correspondences [21]. The state parameter ρ can be computed up to the unknown fixed scale Y as follows

$$\overline{\rho} = \frac{\rho}{Y} = \begin{cases} \sqrt{(E_{12})^2 + (E_{32})^2}\,\cos\phi \, , & \text{if } |\phi| \neq \frac{\pi}{2} \\ \sqrt{(E_{12})^2 + (E_{32})^2}\,\sin\phi \, , & \text{if } |\phi| = \frac{\pi}{2} \end{cases} \tag{37}$$

B. State Observer

In this section, we design a Luenberger observer [26] [27] that improves the performance of the control scheme. The problem of generating an estimate of the state of system is referred to as the problem of designing an observer.

Let the closed-loop of the state system to be defined by $\dot{\mathbf{x}} = \mathbf{g}(\mathbf{x}, \mathbf{u})$. We now define the general observer dynamics

$$\begin{cases} \dot{\hat{\mathbf{x}}} = \mathbf{g}(\hat{\mathbf{x}}, \mathbf{u}) - L(\hat{\mathbf{y}} - \mathbf{y}) \\ \hat{\mathbf{y}} = \mathbf{h}(\hat{\mathbf{x}}) \end{cases} \tag{38}$$

where L is the constant gain of the observer. In the previous section IV-A, we have shown the procedure to estimate the values of ρ, α and ϕ from the essential matrix. However, the estimation of ρ is obtained up to a unknown scale factor. The effect of this issue in the control performance is depicted with two examples in Fig. 7. In the first simulation, the initial location is far from the target, with underestimation of ρ, and it results in low velocities and slow convergence. On the other hand, in the second simulation the initial location is close to the target, with overestimation of ρ, which leads to an oscillating behavior in the orientation of the robot. Although the overdamping behavior showed is stable, this decrease on performance due to the unknown scale factor could lead to instability with higher overestimation of ρ. We will show that an observer on the state variable ρ improves the performance of the control. We focus on this variable particularizing to a reduced-order observer for ρ with

$$\dot{\hat{\rho}} = -k_\rho \hat{\rho} \cos^2\alpha - L_\rho(\hat{y}_\rho - y_\rho) \ , \tag{39}$$

where L_ρ is the gain of the reduced-order observer. The measurement of the variable y_ρ can be defined as a function of the control outputs and the essential matrix entries. The derivatives of the entries of the essential matrix $\mathbf{E}$ with respect to time give

$$\begin{aligned} \dot{E}_{11} &= \dot{E}_{33} = \omega / \cos^2\phi \\ \dot{E}_{12} &= -v/Y - E_{12}E_{33}\omega \\ \dot{E}_{21} &= (v/Y - E_{32}\omega)/\cos\phi \\ \dot{E}_{23} &= E_{12}\omega/\cos\phi \\ \dot{E}_{32} &= -E_{33}v/Y + E_{32}E_{33}\omega \end{aligned} \tag{40}$$

The parameter Y can be solved from the derivative of entry E_{12}. Analogue expressions for Y could be obtained with E_{21} or E_{32}. So, we can compute $Y = -v/(\dot{E}_{12} + E_{12}E_{33}\omega)$ and

$$y_\rho = \overline{\rho}\, Y = \frac{-\overline{\rho}\, v}{\dot{E}_{12} + E_{12}E_{33}\omega} \ , \tag{41}$$

where the value of $\dot{E}_{12}$ is computed with $\dot{E}_{12}(t) = (E_{12}(t) - E_{12}(t - \Delta t))/\Delta t$ and $\overline{\rho}$ is obtained from (37). Denoting $\delta = \dot{E}_{12} + E_{12}E_{33}\omega$, note that (41) becomes singular in particular situations ($\delta = 0$, for example when $\phi = \psi = 0$).

If (39) is subtracted from the system dynamics, and we write $e_\rho = \hat{y_\rho} - y_\rho$, then

$$\begin{cases} \dot{e}_\rho = -\left(k_\rho \cos^2\alpha + L_\rho\right) e_\rho & \text{if } \delta \neq 0 \\ \dot{e}_\rho = -k_\rho \cos^2\alpha \ e_\rho & \text{if } \delta = 0 \end{cases} \tag{42}$$

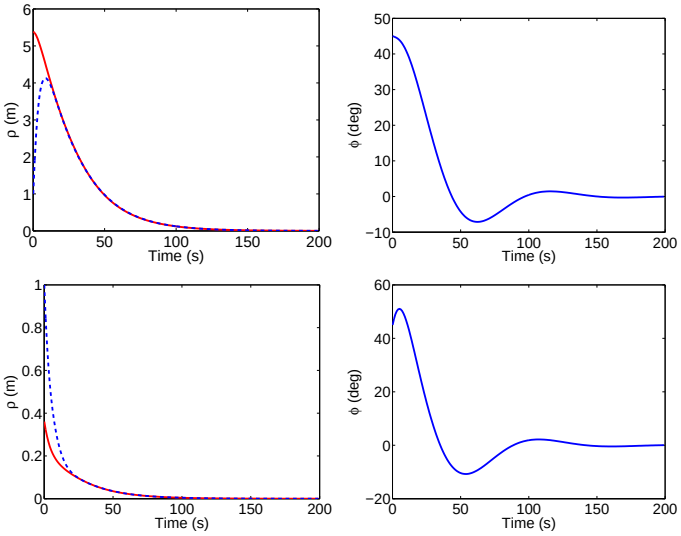

Fig. 8. Simulations with observer for initial positions (x, z, ϕ) at $(-2, 5, 45°)$ (first row) and $(-0.2, 0.3, 45°)$ (second row). Left: Evolution of the real value of ρ (solid line) and the value used in the control (dashed line). Right: Evolution of ϕ. The observer improves the performance (compare with Fig. 7).

Proposition 4.1 (Stability analysis of the observer): The reduced-order observer error dynamics defined in (42) is stable.

Proof: From the previous equations, the dynamic behaviour of the error (42) is asymptotically stable if $\delta \neq 0$, given that $(k_\rho \cos^2\alpha + L_\rho) > 0$ for any $L_\rho > 0$, and (42) is stable if $\delta = 0$ because of $(k_\rho \cos^2\alpha) \geq 0$. So, we conclude that the observer (39) is globally stable. ■

Therefore, stability is guaranteed for the proposed observer but not asymptotic stability. However, we demonstrate in the following section that global asymptotic stability of the control scheme is not compromised. An example of the control scheme with the observer is shown in Fig. 8. Comparison with Fig. 7 shows that the convergence is faster and the control performance improves with the use of the observer.

C. Stability Analysis with Uncertain Parameters

The proposed control law uses the value of the distance to the target location ρ, which is estimated up to unknown fixed scale Y (i.e. ρ_0) assuming that the observer is not used. Next, the stability of the system in the presence of this uncertainty is studied.

Proposition 4.2 (Stability with uncertainty): The closed-loop system (8) with the control gains selected following (13) is globally asymptotically stable despite uncertainty in the state parameter ρ if

$$k_\alpha - k_\phi - k_\rho/\rho_0 > 0 \tag{43}$$

Proof: The following demonstration uses a similar procedure as in Proposition 2.2, but now including the unknown parameter ρ_0 from the estimation of ρ in the computed

velocities (6). The closed loop (8) is then:

$$\begin{aligned}\dot{\rho} &= -\frac{1}{\rho_0}\, k_\rho\, \rho\, \cos^2\alpha \\ \dot{\alpha} &= \frac{1}{\rho_0}\, k_\rho\, \sin\alpha\, \cos\alpha\, -\, k_\alpha\, \alpha + k_\phi\, \phi \\ \dot{\phi} &= -k_\alpha\, \alpha + k_\phi\, \phi \end{aligned} \tag{44}$$

The linear approximation of the system is now

$$\begin{pmatrix} \dot{\rho} \\ \dot{\alpha} \\ \dot{\phi} \end{pmatrix} \approx \begin{bmatrix} -k_\rho/\rho_0 & 0 & 0 \\ 0 & k_\rho/\rho_0 - k_\alpha & k_\phi \\ 0 & -k_\alpha & k_\phi \end{bmatrix} \begin{pmatrix} \rho \\ \alpha \\ \phi \end{pmatrix} \tag{45}$$

Then, the local exponential stability is guaranteed if the selected control gains hold (43).

We define again the Lyapunov function $V(\mathbf{x}) = \mathbf{x}^T\mathbf{P}\mathbf{x} + (k_\rho \sin^2\alpha)/2$ as given in (14) and, following similar steps, we obtain again constraint (13) to guarantee stability properties for all α. Therefore, constraints (43) and (13) are the sufficient conditions for asymptotic stability in the presence of uncertainty in parameter ρ. ■

V. Experimental Validation

In this section we present the experimental evaluation consisting of different simulations and real experiments showing the performance of the proposed control scheme.

A possible choice for the control gains keeping the stability constraints (12) is:

$$k_\rho = 0.03\,, \quad k_\phi = 0.1\,, \quad \text{and} \quad k_\alpha = 0.3\,. \tag{46}$$

This selection fulfil constraints (12) and (13), and the control law with the control gains chosen (46) is globally asymptotically stable. With regard to the uncertainty in parameters, from constraint (43), we have the minimum bound for the uncertainty in ρ_0 is

$$\rho_0 > \frac{k_\rho}{k_\alpha - k_\phi}\,. \tag{47}$$

Using the selection proposed in (46), the asymptotic stability with uncertainty in ρ would be guaranteed if $\rho_0 > 0.03/(0.3-0.1) = 0.15$. Notice in any case that for ρ_0 under 0.15, the stability region is still enlarged in practice by using the observer previously presented.

The simulated scene consists of a cloud of 3D points randomly distributed. The set of points are projected into the camera image plane (size 640×480 pixels) to obtain the point correspondences used to compute the essential matrix and subsequently the velocities for the motion are computed by the control law. Simulations from different initial locations are depicted in Fig. 9. showing successful convergence of the system.

We have defined the calibration matrix of the general pinhole camera model as

$$\mathbf{K} = \begin{bmatrix} f\,m_x & s & x_0 \\ 0 & f\,m_y & y_0 \\ 0 & 0 & 1 \end{bmatrix} = \begin{bmatrix} 640 & 0 & 0 \\ 0 & 480 & 0 \\ 0 & 0 & 1 \end{bmatrix}, \tag{48}$$

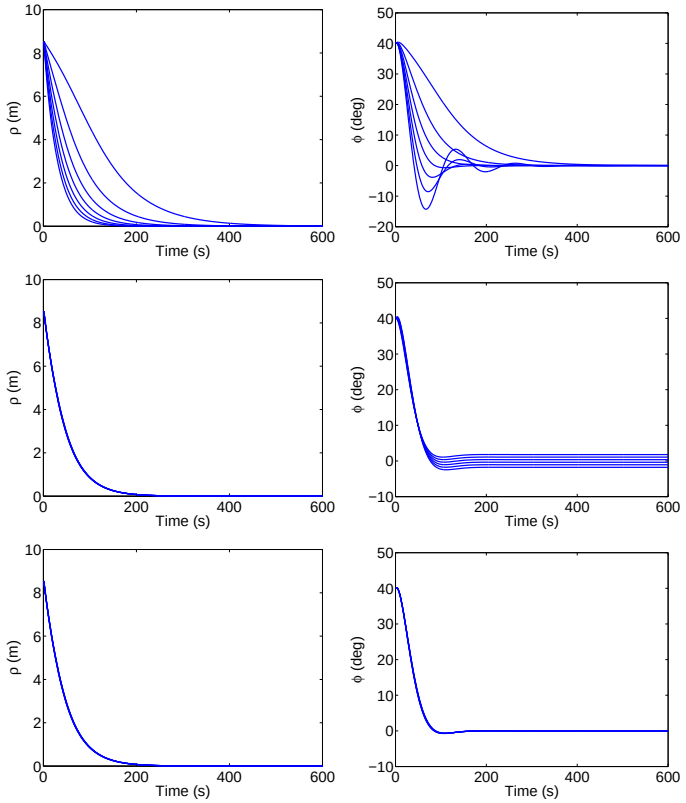

Fig. 10. Evolution of ρ (left) and ϕ (right) in the presence of calibration errors. Each graphic depicts a set of simulations with varying parameters: focal length (first row), x_0 (second row), and y_0 (third row).The initial location in these simulations is $(x, z, \phi) = (3, -8, 40°)$.

where f is the focal length of the camera and m_x, m_y are the pixels per distance unit in the x and y directions respectively; s is the skew parameter and $(x_0,\, y_0)$ are the coordinates of the principal point. The estimation of the essential matrix requires the internal camera calibration. Thus, we test the performance of the control law associated with the uncertainty of the camera calibration parameters. The values of $\mathbf{K}$ have been fixed to (48), while the values known by the controller in the simulations of Fig. 10 are changed. The value of the focal length is changed from 3 to 9 mm for a real value of 6 mm. It can be seen in Fig. 10 (first row) that the variation of f only affects to the convergence time. The principal point coordinates are changed from -10 to 10 pixels for a real value of 0 pixels. The variation of x_0 does not affect to the convergence except a final error in the orientation, as shown in Fig. 10 (second row). For example an error in x_0 of 10 pixels yields to an error in the final orientation of -1.79 deg. The system converges to the goal with any variation on y_0, (the resultant plots are superposed in Fig. 10 (third row)). Thus, assuming usual uncertainties in the camera calibration parameters, the final location errors can be disregarded.

In the real experiments, the mobile robot used is a Pioneer P3-DX from ActivMedia, Fig. 11. The robot is equipped with a Point Grey Research Flea2 camera mounted on top and

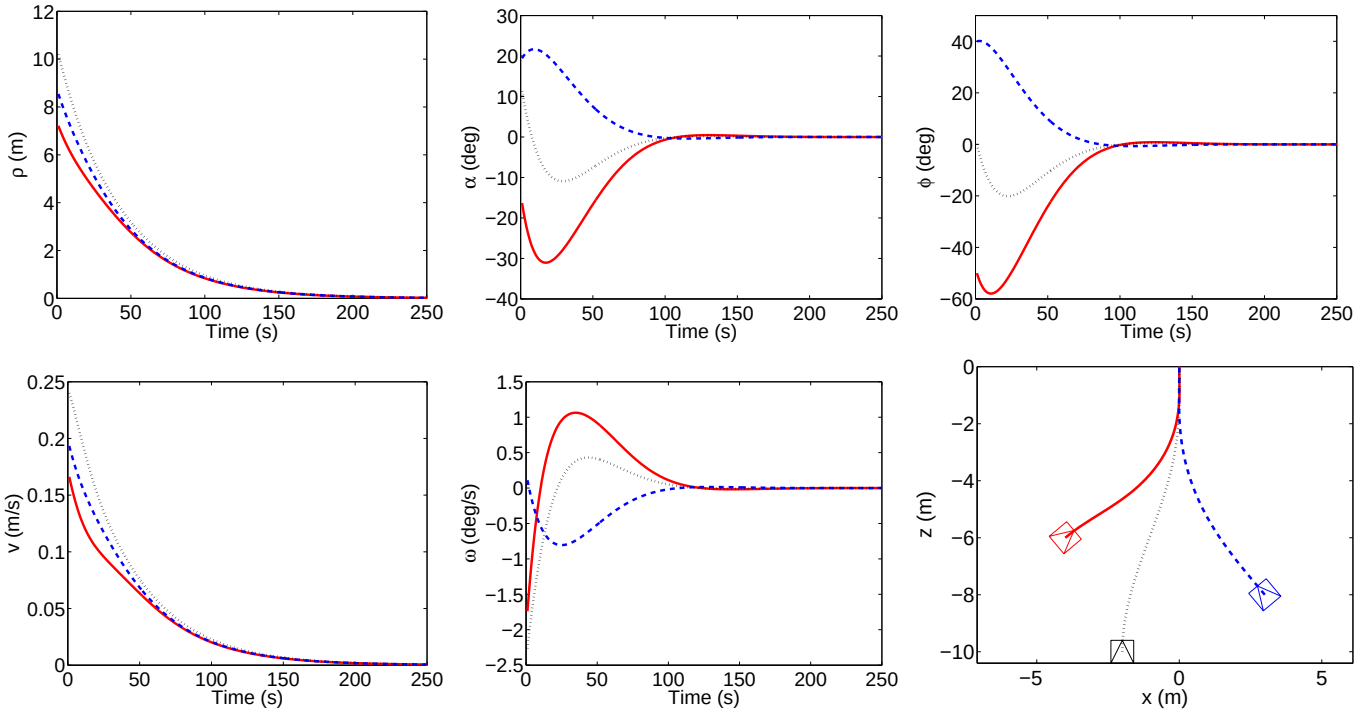

Fig. 9. Simulations for three different initial positions. The target location is $(0, 0, 0^\circ)$ and the initial locations are $(x, z, \phi) = (-4, -6, -50^\circ)$ with solid line, $(x, z, \phi) = (-2, -10, 0^\circ)$ with dotted line, and $(x, z, \phi) = (3, -8, 40^\circ)$ with dashed line. The evolution of the system state (ρ, α, ϕ) is depicted (first row), as well as the output velocities (v, ω) and a top view of the robot motion (second row).

forward looking. Notice that the field-of-view constraints of the visual sensor are not taken into account specifically in the approach presented. In order to ensure keeping the features of interest in the field of view during the robot control, the standard camera can be replaced with an omnidirectional one without any modification of the control scheme. For simplicity, we use here a standard camera rather than an omnidirectional one. The camera is connected to a laptop onboard the robot (Intel® Core^{TM} 2 Duo CPU at 2.50 GHz). The images are acquired at size 600×800, and an example of images taken during one of the experiments is shown in Fig. 12. The putative matches have been obtained using the Lucas and Kanade tracking algorithm [28], [29]. The presence of image noise or mismatches needs to be assumed and we use the RANSAC method [30] to reject wrong matches. The point correspondences obtained after the robust estimation of the essential matrix are depicted in Fig. 12 (left). The middle image in Fig. 12 shows the virtual points computed to define the virtual target. The evolution of the tracked points on the image plane during the motion of the platform are shown in Fig. 12 (right).

The results of three different real experiments are depicted in Fig. 13. The acquired image data is processed using the OpenCV library (www.intel.com). The velocities computed are sent to the robot, at a rate of 12 Hz, through the serial port using the ARIA library (www.activrobots.com). In each row of Fig. 13, the computed velocities and the resultant evolution of the robot for three different initial locations are depicted.

Fig. 11. The experimental platform, a Pioneer P3-DX from ActivMedia.

The final error measured is around several centimeters. The results obtained from the experiments carried out show the performance of the proposal. The control performance is subordinated to the obtention of a minimum set of correspondences between the current and target images. Otherwise, the essential matrix cannot be estimated, leading to failure of the control. On the other hand, the geometric constraint imposed through the essential matrix increases the robustness of the system to spurious putative matches or image noise.

VI. Conclusion

We have presented a new vision-based control approach for the stabilization of mobile robots. The contribution is a control scheme with an observer that relies on visual information provided through the essential matrix. The evolution of the

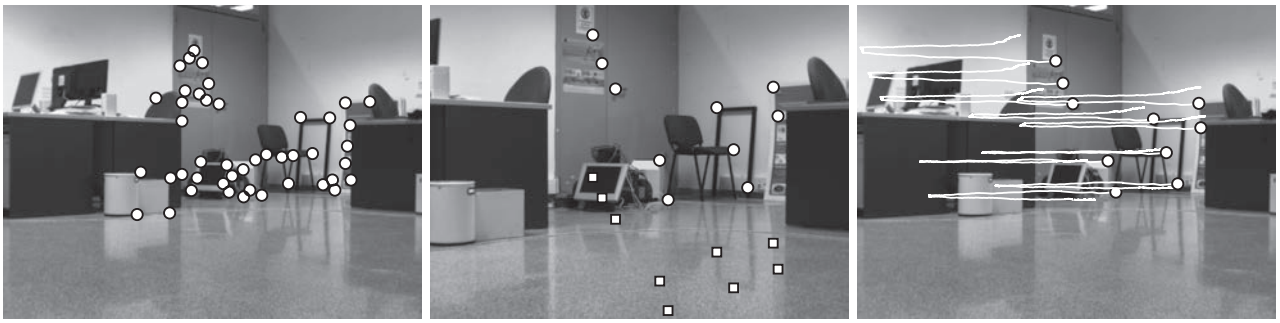

Fig. 12. Left: Initial image of an experiment with the point features detected. Middle: Target image with the points matched (circles) and the computed virtual target points (squares). Only ten points are depicted for clarity. Right: Trajectories of the points in the image tracked during the navigation (only ten are depicted).

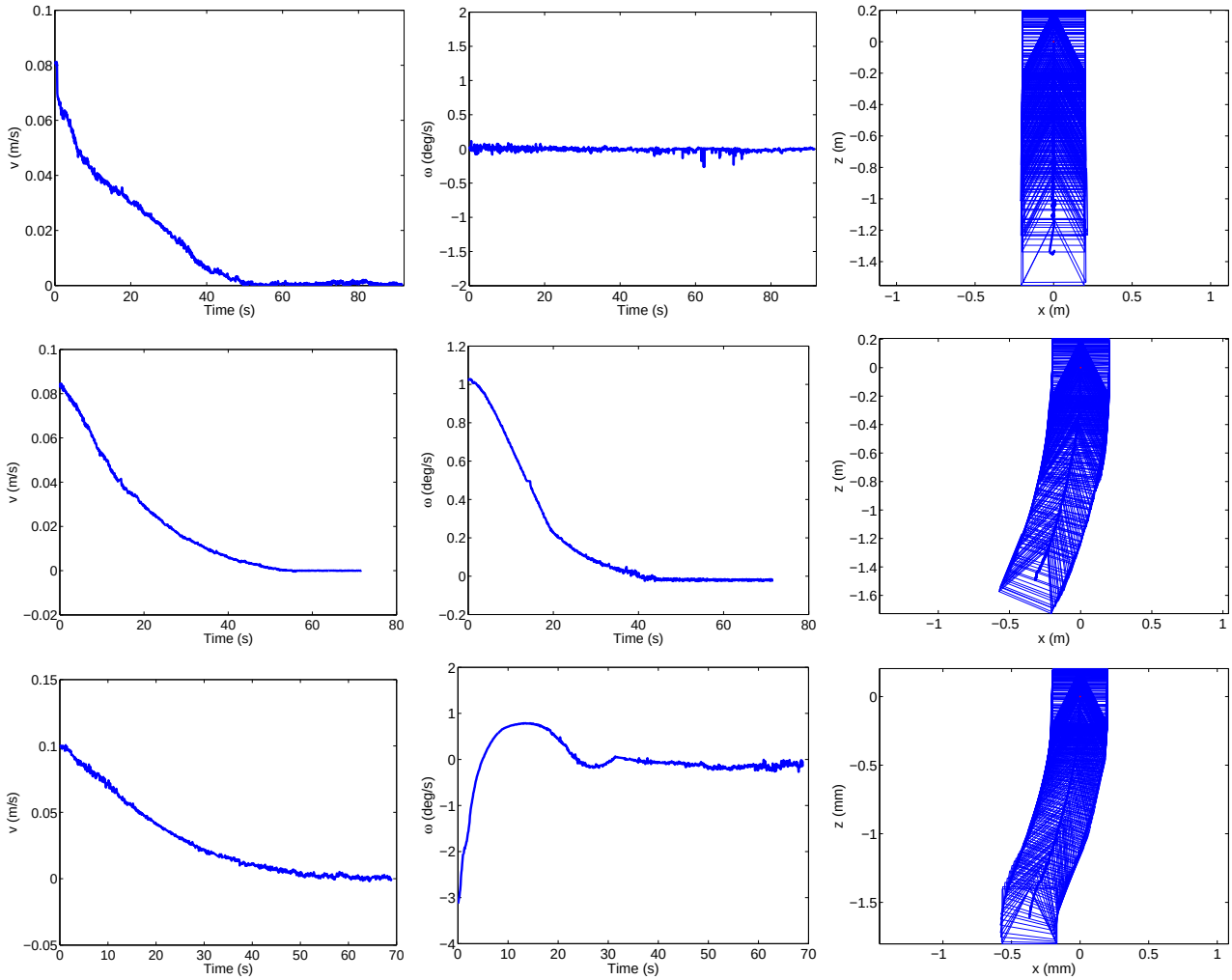

Fig. 13. Experiments with the real platform. Three experiments are shown, one per row.The output velocities (v, ω) are depicted (left and middle columns) and a top view of the robot motion (right column).

system under our control scheme has been shown to be globally asymptotically stable. This approach overcomes the critical issue of the essential matrix degeneracies with short baseline by means of a virtual target. The experimental evaluation consists of simulations and real experiments showing the performance of the proposal. The proposed scheme requires part of the scene to be shared by the current and target images in order to find enough matches for computing the essential matrix. Although we have used a standard camera in the experiments, an omnidirectional camera can be used directly in the same way to overcome field-of-view constraints.

ACKNOWLEDGMENT

This work was supported by projects DPI2009-08126 and DPI2009-14664-C02-01 of the "Ministerio de Ciencia e Innovación, Gobierno de España".

REFERENCES

[1] F. Chaumette and S. Hutchinson, "Visual servo control, part I: Basic approaches," *IEEE Robotics and Automation Magazine*, vol. 13, no. 4, pp. 82–90, Dec. 2006.

[2] G. Chesi and K. Hashimoto, *Eds. Visual Servoing via Advanced Numerical Methods*. Lecture Notes in Control and Information Sciences, Vol. 401, Springer-Verlang, 2010.

[3] C. Canudas de Wit and O. J. Sordalen, "Exponential stabilization of mobile robots with nonholonomic constraints," *IEEE Transactions on Automatic Control*, vol. 37, no. 11, pp. 1791–1797, 1992.

[4] M. Aicardi, G. Casalino, A. Bicchi, and A. Balestrino, "Closed loop steering of unicycle like vehicles via lyapunov techniques," *IEEE Robotics & Automation Magazine*, vol. 2, no. 1, pp. 27–35, Mar. 1995.

[5] G. Indiveri, "Kinematic time-invariant control of a 2D nonholonomic vehicle," in *IEEE Conference on Decision and Control*, vol. 3, 1999, pp. 2112–2117.

[6] A. Astolfi, "Exponential stabilization of a wheeled mobile robot via discontinuous control," *Journal of Dynamic Systems, Measurement, and Control*, vol. 121, no. 1, pp. 121–126, Mar. 1999.

[7] F. Conticelli, B. Allotta, and P. Khosla, "Image-based visual servoing of nonholonomic mobile robots," in *IEEE Conference on Decision and Control*, vol. 4, 1999, pp. 3496–3501.

[8] M. O. Franz, B. Schölkopf, H. A. Mallot, and H. H. Bülthoff, "Learning view graphs for robot navigation," *Autonomous Robots*, vol. 5, no. 1, pp. 111–125, 1998.

[9] A. A. Argyros, K. E. Bekris, S. C. Orphanoudakis, and L. E. Kavraki, "Robot homing by exploiting panoramic vision," *Autonomous Robots*, vol. 19, no. 1, pp. 7–25, 2005.

[10] R. Basri, E. Rivlin, and I. Shimshoni, "Visual homing: Surfing on the epipoles," *International Journal of Computer Vision*, vol. 33, no. 2, pp. 117–137, 1999.

[11] P. Rives, "Visual servoing based on epipolar geometry," in *Int. Conference on Intelligent Robots and Systems*, vol. 1, 2000, pp. 602–607.

[12] G. Chesi and K. Hashimoto, "A simple technique for improving camera displacement estimation in eye-in-hand visual servoing," *IEEE Transactions on Pattern Analysis and Machine Intelligence*, vol. 26, no. 9, pp. 1239–1242, Sept. 2004.

[13] G. López-Nicolás, C. Sagüés, J. J. Guerrero, D. Kragic, and P. Jensfelt, "Switching visual control based on epipoles for mobile robots," *Robotics and Autonomous Systems*, vol. 56, no. 7, pp. 592–603, 2008.

[14] S. Benhimane, E. Malis, P. Rives, and J. R. Azinheira, "Vision-based control for car platooning using homography decomposition," in *Int. Conf. on Robotics and Automation*, April 2005, pp. 2173–2178.

[15] Y. Fang, W. E. Dixon, D. M. Dawson, and P. Chawda, "Homography-based visual servo regulation of mobile robots," *Trans. on Systems, Man, and Cybernetics, Part B*, vol. 35, no. 5, pp. 1041–1050, 2005.

[16] J. Chen, W. Dixon, M. Dawson, and M. McIntyre, "Homography-based visual servo tracking control of a wheeled mobile robot," *IEEE Transactions on Robotics*, vol. 22, no. 2, pp. 406–415, April 2006.

[17] S. Benhimane and E. Malis, "Homography-based 2D visual servoing," in *Int. Conf. on Robotics and Automation*, 2006, pp. 2397–2402.

[18] J. Courbon, Y. Mezouar, and P. Martinet, "Indoor navigation of a non-holonomic mobile robot using a visual memory," *Autonomous Robots*, vol. 25, no. 3, pp. 253–266, 2008.

[19] G. López-Nicolás, N. R. Gans, S. Bhattacharya, J. J. Guerrero, C. Sagüés, and S. Hutchinson, "Homography-based control scheme for mobile robots with nonholonomic and field-of-view constraints," *IEEE Transactions on Systems, Man, and Cybernetics, Part B*, vol. 40, no. 4, pp. 1115–1127, 2010.

[20] E. Malis and F. Chaumette, "2 1/2 D visual servoing with respect to unknown objects through a new estimation scheme of camera displacement," *International Journal of Computer Vision*, vol. 37, no. 1, pp. 79–97, 2000.

[21] R. I. Hartley and A. Zisserman, *Multiple View Geometry in Computer Vision*, 2nd ed. Cambridge University Press, 2004.

[22] D. Nister, "An efficient solution to the five-point relative pose problem," in *IEEE Computer Society Conference on Computer Vision and Pattern Recognition*, vol. 2, June 2003, pp. 195–202.

[23] G. López-Nicolás, C. Sagüés, and J. J. Guerrero, "Parking with the essential matrix without short baseline degeneracies," in *IEEE International Conference on Robotics and Automation*, May 2009, pp. 1098–1103.

[24] R. W. Brockett, "Asymptotic stability and feedback stabilization," in *Differential Geometric Control Theory*. Birkhauser, Boston, USA, R. W. Brockett, R. S. Millmann and H. J. Sussmann, Eds., 1983, pp. 181–191.

[25] H. K. Khalil, *Nonlinear Systems*, 3rd ed. Prentice Hall, 2001.

[26] D. G. Luenberger, "Observing the state of a linear system," *IEEE Transactions Military Electronics*, vol. MIL-8, pp. 74–80, Apr. 1964.

[27] F. E. Thau, "Observing the state of nonlinear dynamic systems," *International Journal of Control*, vol. 17, no. 3, pp. 471–479, Mar. 1973.

[28] J. Shi and C. Tomasi, "Good features to track," *IEEE Computer Society Conference on Computer Vision and Pattern Recognition*, pp. 593–600, June 1994.

[29] B. D. Lucas and T. Kanade, "An iterative image registration technique with an application to stereo vision," in *Proc. of 7th International Joint Conference on Artificial Intelligence (IJCAI)*, 1981, pp. 674–679.

[30] M. A. Fischler and R. C. Bolles, "Random sample consensus: a paradigm for model fitting with applications to image analysis and automated cartography," *Commun. ACM*, vol. 24, no. 6, pp. 381–395, 1981.